Dynamical thermal behavior and thermal self-stability of microcavities

Tal Carmon, Lan Yang, and Kerry J. Vahala

Department of Applied Physics, California Institute of Technology, Pasadena, California 91125
tal@caltech.edu

Abstract: As stability and continuous operation are important for almost any use of a microcavity, we demonstrate here experimentally and theoretically a self-stable equilibrium solution for a pump-microcavity system. In this stable equilibrium, intensity- and wavelength-perturbations cause a small thermal resonant-drift that is enough to compensate for the perturbation (noises); consequently the cavity stays warm and loaded as perturbations are self compensated. We also compare here, our theoretical prediction for the thermal line broadening (and for the wavelength hysteretic response) to experimental results.

OCIS codes: (140.4780) Optical resonators; (190.1450) Bistability; (140.3410) Laser resonators; (140.6810) Thermal effects.

References and links

1. V. B. Braginsky, M. L. Gordetsky and V. S. Ilchenko, "Quality-factor and nonlinear properties of optical whispering-gallery modes," Phys. Lett. A **137**, 393 (1989)
2. V.S. Ilchenko, M.L. Gorodetsky, X.S. Yao, and L. Maleki, "Microtorus: a high-finesse microcavity with whispering-gallery modes," Opt Lett **26**, 256, (2001).
3. D. K. Armani, T. J. Kippenberg, S. M. Spillane & K. J. Vahala, ""Ultra-high-Q toroid microcavity on a chip"," Nature **421**, 925 (2003).
4. M.L. Gorodetsky, and V.S. Ilchenko, "Optical microsphere resonators: optimal coupling to high-Q whispering-gallery modes," J. Opt. Soc. Am. B. **16**, 147 (1999).
5. B.E. Little, J. P. Laine, H.A. Haus. "Analytic theory of coupling from tapered fibers and half-blocks into microsphere resonators," J. Lightwave Technol. **17**, 704 (1999).
6. V. B. Braginsky, Y.I. Vorontsov, and K.S. Thorne, "Quantum non-demolition measurements," Science, **209**, 47 (1980).
7. V. B. Braginskii, and V. S. Il'chenko, Dokl. Akad. Nauk SSSR, **293**, 1358 (1987).
8. D. F. Walls and G. Milburn, *Quantum Optics*, (Springer, New York, 1994).
9. M. Scully and M. Zubairy, *Quantum Optics*, (Cambridge,1996).
10. Bouwmeester, A. Ekert, and A. Zeilinger, "The Physics of Quantum Information," (Heidelberg, 2000).
11. S. M. Spillance, T. J. Kippenberg and K. J. Vahala, "Ultralow-threshold Raman laser using a spherical dielectric microcavity," Nature, **415**, 621 (2002).
12. S. L. McCall, A. F. J. Levi, R. E. Slusher, S. J. Pearton, and R. A. Logan, "Whispering-gallery mode microdisk lasers," Appl. Phys. Lett. **60**, 289–291 (1992).
13. F. Treussart, J. Hare, V. Lefèvre-Seguin, J. -M. Raimond, and S. Haroche. "Very low threshold whispering-gallery-mode microsphere laser," Phys. Rev. A **54**, R1777–R1780 (1996).
14. Lan Yang, D. K. Armani, and K. J. Vahalab, "Fiber-coupled Erbium Microlasers on a chip," Appl. Phys. Lett, **83**, 825 (2003).
15. T. J. Kippenberg, S. M. Spillane and K. J. Vahala, "Kerr-nonlinearity induced optical parametric oscillation in a ultra-high-Q toroid microcavity ," Phys. Rev. Lett. **93**, 083904 (2004).
16. V. Lefevre-Seguin, and S. Haroche, "Towards cavity-QED experiments with silica microspheres," Mater. Sci. Eng. B **48**, 53–58 (1997).
17. D.W. Vernooy, A. Furusawa, N. P. Georgiades, , V. S. Ilchenko, and H. J. Kimble, "Cavity QED with high-Q whispering gallery modes," Phys. Rev. A **57**, R2293–R2296 (1998).
18. F. Vollmer, D. Braun, A. Libchaber, M. Khoshsima, I. Teraoka, and S. Arnold. "Protein detection by optical shift of a resonant microcavity," Appl. Phys. Lett. **80**, 4057–4059 (2002).
19. A. Serpenguzel, S. Arnold, and G. Griffel, "Excitation of resonances of microspheres on an optical fiber," Opt. Lett. **20**, 654–656 (1995).
20. R. K. Chang, and A. J. Campillo, *Optical Processes in Microcavities*, (World Scientific, Singapore, 1996).

#4672 - $15.00 US Received 17 August 2004; revised 16 September 2004; accepted 17 September 2004

21. V. S. Ilchenko, and M. L. Gorodetskii, "Thermal nonlinear effects in optical whispering gallery microresonators," Laser Phys. **2**, 1004 (1992).
22. F. Treussart, V.S. Ilchenko, J.-F. Roch, J. Hare, V. Lefèvre-Seguin, J.-M. Raimond, - S. Haroche. "Evidence for intrinsic Kerr bistability of high-Q microsphere resonators in superfluid helium," Eur. Phys. J. D. **1**, 235–238 (1998).
23. To be precise, while heat convection is proportional to the surface area (l^2), heat conduction is proportional to the area divided by the pass length ($l^2/l = l$). Since both convection and conduction contribute here, the precise scaling is $\Delta T \propto l \div l^2$. Being very precise, one should also consider the fact that light wavelength is usually not scaled down and hence the mode volume scaling is actually slightly smaller than l^3.
24. David N. Nikogosyan, *Properties of Optical and Laser Related Materials A Handbook*, (John Wiley & Son, 1997).
25. M. L. Gorodetsky, and I. S. Grudinin, "Fundamental thermal fluctuations in microspheres," J. Opt. Soc. Am. B **21**, 697, (2004).
26. In this case one should use:
$$Cp_1 \Delta\dot{T}_1(t) = I_h \frac{1}{\left(\frac{\lambda_p - \lambda_0 (1 + a(\Delta T_1(t) + \Delta T_2(t)))}{\Delta\lambda / 2}\right)^2 + 1} - K_1 \Delta T_1(t)$$
$$Cp_2 \Delta\dot{T}_2(t) = K_1 \Delta T_1(t) - K_2 \Delta T_2(t),$$
where the first equation describes heat dissipation from the mode volume to the cavity structure and the second equation describes heat dissipation from the cavity structure to the surrounding. Here Cp_1 is the thermal capacity of the mode volume, Cp_2 is the thermal capacity of the cavity structure, K_1 is the thermal conductivity between the mode volume and the rest of the cavity, K_2 is the thermal conductivity between the cavity and the surrounding, ΔT_1 is the temperature difference between the mode volume and the rest of the cavity and ΔT_2 is the temperature difference between the cavity and the surrounding.
27. T. Carmon, T. J. Kippenberg, L. Yang, H. Rokhsari, S. Spillane, K., J, Vahala, "Power locked and wavelength locked ultra-high-Q optical microcavities," Submitted to Appl. Phys. Lett. (Aug, 2004).

1. Introduction

As spherical cavities [1] and toroidal cavities [2,3] composed of silica offer low optical losses (high Q factors) together with mode volume as small as $\sim 100\lambda^3$ and negligible pump-device coupling-losses [4,5]; they possess a superb figure of merit for study of a diverse set of optical phenomena. This includes quantum-nondemolition measurements [6,7], generation of non-classical states [8,9], quantum information research [10], Raman scattering [11], lasing [12-14], parametric oscillation [15], cavity quantum electrodynamics [16,17], biosensing [18,19] and other optical effects [20]. However, small mode volume also makes these devices susceptible to thermal induced nonlinearities [21]. This is because power lost through absorption within the down-scaled resonator must now dissipate through a smaller surface area. As a result cavity heating cannot be neglected and the thermal drift of the cavity optical resonance can easily exceed 100 cavity linewidths. A wide range of thermal-induced phenomena such as hysteretic wavelength response [1,22] and oscillatory instability [21] were experimentally reported, however, this behavior was not modeled into a dynamical formula before as far as is known to the authors. In addition, for most applications of microcavities, including all of the above cited applications, [6-22], a frequency-stable operation is desirable in the presence of thermal instability.

Here we formulate the dynamical thermal behavior for microcavity systems. The equations of motion explain hysteretic wavelength response, thermal line broadening and the existence of equilibrium solutions, one of which is particularly important because it is self stable. When operating in the self-stable regime the system automatically corrects for drifts and deviations. We verify experimentally each of the above theoretical predictions. In particular, we demonstrate theoretically and experimentally a method for self-stabilization based upon thermal nonlinearity.

2. Microcavity dynamical thermal-behavior

A simple scaling argument explains why thermal effects are immaterial when using large cavities, however, cannot be neglected when using microcavities. Down scaling has the side

#4672 - $15.00 US Received 17 August 2004; revised 16 September 2004; accepted 17 September 2004

effect of a temperature increase, ΔT (relative to the ambient temperature) which scales as $\Delta T \propto 1/l^2$. This is because heat goes out of the cavity through the surface area, which is now l^2 smaller [23]. Scaling down the cavity size will also make the thermal time constant (t_{th}) faster as the first power of down scaling ($t_{th} \propto l$). This is because the thermal response time is proportional to the heat capacity divided by the heat conductivity. As the thermal effects become larger and faster with the down scaling, the temperature change induces a change in the cavity optical path (through the thermal expansion coefficient and the thermal change of the refractive index).

The reason for making smaller microcavities is the fact that the figure of merit for most optical process is scaled inversely with the mode volume. Here we will address the temperature increase that results by this cavity downscaling. We will first formulate the governing dynamical thermal-equation for the microcavity. Afterwards we will search for steady state solutions in which there is a stable balance between the heat that goes into the cavity and the heat that goes out of the cavity.

When the cavity medium has an expansion coefficient of ε (units: $m/(m^0 C)$) and refractive index temperature coefficient of dn/dT (units: $1/^0 C$) it follows that the N-th resonant wavelength (λ_r) must obey:

$$N = \frac{2\pi r c_1 (1+\varepsilon \Delta T)}{\lambda_r /(n_0 + \frac{dn}{dT}\Delta T)} \tag{1}$$

where *r* is the cavity radius, c_1 contains the waveguide propagation-constant and the fact that the light rotation-radius is slightly smaller than the cavity radius; n_0 is the cavity index of refraction and ΔT is the temperature difference between the mode volume and the surrounding. We extract the resonance wavelength as a function of the temperature to obtain

$$\begin{aligned} \lambda_r(\Delta T) &\cong \lambda_0 [1 + (\varepsilon + \frac{dn}{dT}/n_0)\Delta T] \\ &\equiv \lambda_0 (1 + \quad a \quad \Delta T). \end{aligned} \tag{2}$$

Here λ_0 is the cold cavity resonance-wavelength. For simplicity, we now define a temperature coefficient of resonance-wavelength, $a \equiv \varepsilon + \frac{dn}{dT}/n_0$, which contains both thermal expansion and the thermal index change. For fused silica we calculate the temperature coefficient of the resonance-wavelength to be $a = 6 \cdot 10^{-6} [1/^0 C]$[24]. The quadratic temperature dependence in the above expression is negligible in our case.

Heat that flows into the cavity is a function of (i) the pump power (*I*), (ii) the optical power coupling efficiency (η), (iii) the fact that only losses due to optical absorption (i.e., as opposed to scattering) take part in warming the cavity, and (iv) the deviation of the pump wavelength (λ_p) from the thermally-drifted Lorentzian lineshape of the cavity [4]. The net heat flow [J/second] into the cavity is therefore:

$$\dot{q}_{in} = I\,\eta\,\frac{Q}{Q_{abs}}\,\frac{1}{\left(\frac{\lambda_p - \lambda_r}{\Delta\lambda/2}\right)^2 + 1} \equiv \quad I_h \quad \frac{1}{\left(\frac{\lambda_p - \lambda_0\,(1 + a\,\Delta T)}{\Delta\lambda/2}\right)^2 + 1} \tag{3}$$

Here Q_{abs} is the cavity quality factor due to absorption losses only (since scattered light does not heat the cavity) and $\Delta\lambda$ is the resonance bandwidth ($Q = \lambda_0/\Delta\lambda$). In the second row of this equation we define the power that actually heats the cavity as $I_h \equiv I\,\eta\,Q/Q_{abs}$ and also use the temperature dependent expression for λ_r as describes in Eq. (2).

#4672 - $15.00 US Received 17 August 2004; revised 16 September 2004; accepted 17 September 2004

From energy conservation, the net heat to the cavity is the heat that goes in ($\dot{q}_{in}$) minus the heat that goes out ($\dot{q}_{out}$):

$$Cp\,\Delta\dot{T}(t) = \dot{q}_{in} - \dot{q}_{out} = I_h \frac{1}{\left(\frac{\lambda_p - \lambda_0 (1 + a\,\Delta T)}{\Delta\lambda/2}\right)^2 + 1} - K\Delta T(t)^{\cdot} \quad (4)$$

Here *Cp* is the heat capacity ($J/^0C$) and K ($J/(s^0C)$) is the thermal conductivity between the cavity mode volume and the surrounding. Various sources of noise, such as microcavity thermorefractive noise [25], pump fluctuations and others can now incorporated into equation 4 to test their influence.

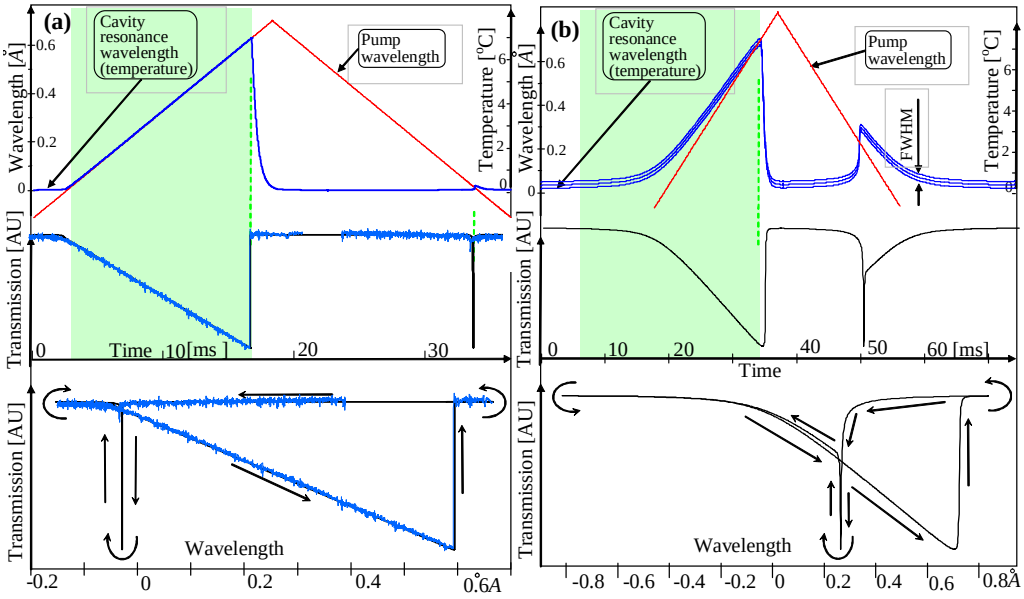

Fig. 1. Dynamical thermal behavior of a toroidal microcavity (a) As the pump makes a $46\,\mathring{A}/s$ wavelength scan (upper red) it approaches the cavity resonance (upper blue) and cause a thermal drift of the resonance line. In the upper plot, the right ordinate describes the temperature of the mode volume relative to the ambient temperature and the left ordinate gives the pump wavelength and cavity resonance wavelength (relative to the cold resonance). The pump-cavity transmission is presented as a function of time (middle) and as a function of the pump wavelength (bottom). Here blue dots represent experimentally measured data and lines stand for calculations. The parameters used for the fit are $I_h/K = 7.16^oC$ and $I_h/Cp = 18000\ ^oC/s$. The cold resonance wavelength of the microcavity is $\lambda_0 = 1545nm$ and its quality factor is $Q = 2\times10^7$, the pump power was 1.8 mW. (b) To emphasize fine details, we repeat the same calculation but using a reduced Q ($Q = 5\times10^5$), For convenience, the cavity FWHM is marked on the cavity resonance wavelength (top blue).

We note here that the most precise description for this system is provided by the 3D Laplacian heat-transfer equation in which I and ΔT are functions of time and spatial coordinates (t,x,y,z) and K, *Cp* are functions of spatial coordinates (x,y,z). Il'chenko [21], however, points out that there are two types of thermal nonlinearities, a faster one connected with heat dissipation from the mode volume to the remainder of the microcavity structure and a slower one connected with heat dissipation from the microcavity to the surrounding. Typically, (for a sphere with diameter=0.14 mm) the fast mechanism response time is a few microseconds while the slow mechanism response time is tens of milliseconds. The fast

#4672 - $15.00 US Received 17 August 2004; revised 16 September 2004; accepted 17 September 2004

mechanism index-change is about 3 percent of the slow mechanism. Considering this, when treating a system over a broad range of time scales we would need to split Eq. (4) into two parts [26]. This two-stage treatment, together with other high order effects, such as the cavity charging time ($\tau = Q/\omega$), coupling between different modes, Kerr nonlinearity, and stress induced index change will not be treated here.

We will now examine the cavity dynamical thermal-behavior (Eq. (4)) by comparing the experimentally measured cavity transmission during a wavelength scan to the calculated transmission. As we will show below, for the time scales presented in this paper, Eq (4) properly describes our cavity thermal behavior. In Fig 1(a) we present the measured transmission together with the calculated cavity transmission, cavity temperature and cavity resonant wavelength during up and down wavelength scans of the pump laser. The fit parameters for the calculation were the heat capacity and heat conduction (normalized to the absorbed power); these parameters are comparable with a simple calculation based on cavity dimensions and thermal properties.. We see in Fig 1(a) that as the pump wavelength approaches the cavity tail (at $t = 2ms$) the cavity starts to heat up. As a result, the cavity resonance wavelength drifts away from the pump wavelength ($t = 2\frac{0}{0}16ms$). The cavity temperature rise terminates when the pump wavelength reaches the center of the drifted absorption line ($t = 16ms$). At this point, the absorption is maximal and cannot increase further to compensate for heat dissipation. Beyond this point, the pump cannot push the cavity resonance further and the resonance is lost as it quickly drifts down. Later, when the pump wavelength begins the backward scan ($t = 19ms$) it meets the cavity resonance again but at this time from the other direction. The cavity resonance then ($t = 32ms$) quickly flips sides with the pump yielding a hysteretic response.

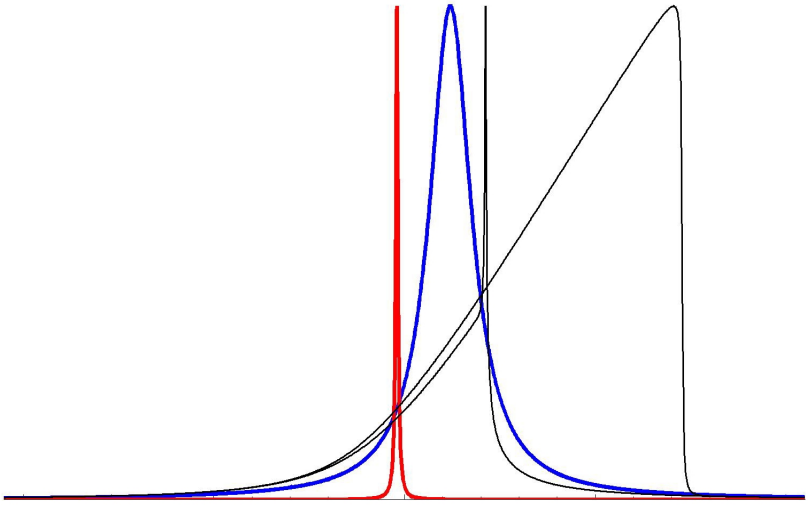

Fig. 2. (2.4 MB) Movie of the cavity wavelength response (6.6 MB version). The scanning-pump (red) induces thermal drift of the resonant lineshape (blue). The intersection point between the pump line and the cavity Lorentzian draws the hysteretic absorption (black). Parameters here are identical to the parameters in Fig. 1(b). The movie is in slow motion as each scan cycle truly takes 80 *ms*

The back-scan measured transmission does not go to minimum because of the scan rate across the cavity lineshape is sufficiently fast to prevent full "charging" of the resonator. The hysteretic behavior of the cavity results from the fact that the resonance wavelength will always shift upward when approached by the pump. No matter whether the resonance is approached (by the pump) from high wavelength or from low wavelength sides, the resonance

#4672 - $15.00 US Received 17 August 2004; revised 16 September 2004; accepted 17 September 2004

will always drift to the high wavelength! This hysteretic behavior is best exemplified in Fig 2 (multimedia).

3. Steady state solutions

In steady state there is an equilibrium between the absorbed- and dissipated-heat. If this balance is a stable equilibrium, then the cavity can operate continuously in that regime and overcome perturbations (as for example are caused by power- and wavelength-perturbation of the pump). On the contrary, if the equilibrium is an unstable one, the smallest perturbation will lead to temperature change that will take the system far away from this equilibrium. We will investigate the equilibrium solutions for Eq. (4):

$$0 = I_h \frac{1}{\left(\frac{\lambda_p - \lambda_0 (1 + a \Delta T)}{\Delta\lambda / 2} \right)^2 + 1} - K \Delta T \quad . \tag{5}$$

As Eq. (5) is cubic in ΔT , it has one to three equilibrium solutions (for a given pump power).

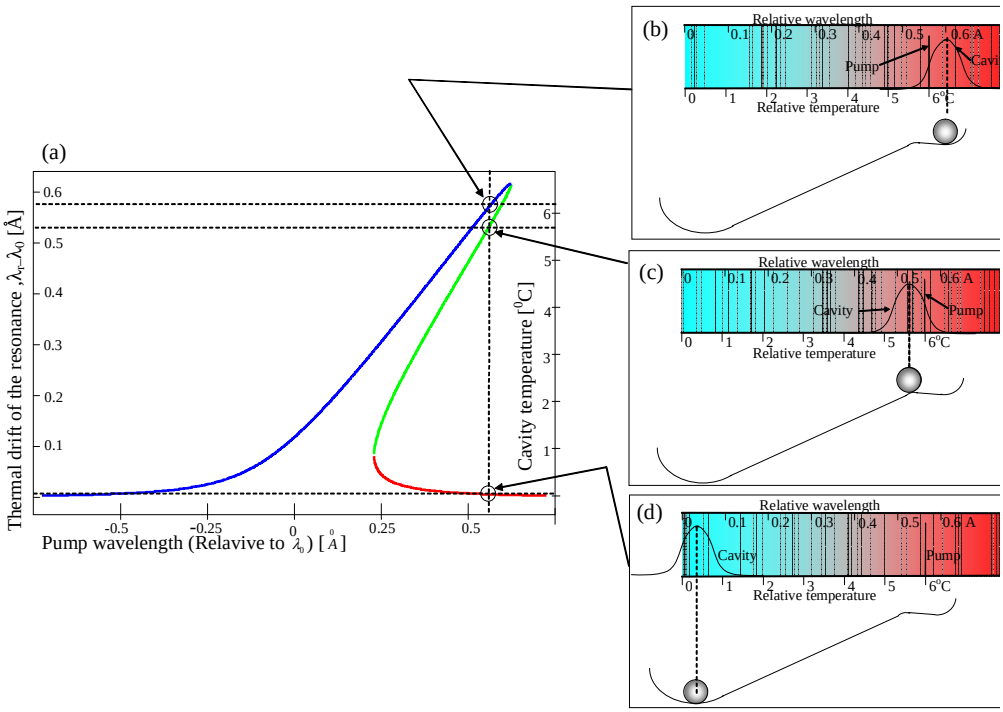

Fig. 3 Equilibrium solutions: (a) Presented are the resonant thermal wavelength-drift (left ordinate) and the cavity temperature (right ordinate, relative to the ambient temperature) at equilibrium for various values of pump wavelength (horizontal axis). The 3 distinct equilibrium regimes are color coded. On the right (b, c, and d), we illustrate a solution-triplet for the pump position shown in the left panel. (Parameters are as in Fig. 1(b))

These solutions are drawn in Fig 3 for various values of pump wavelength (λ_p). We can see in Fig. 3, that as the pump wavelength increases, the number of equilibrium solutions goes from 1 to 3 (and then back to 1). Consider as an example a pump wavelength shifted by 0.56 angstrom relative to the cold-cavity resonance. The corresponding equilibrium thermal drift of the resonance can be either 0.58, 0.52 or 0.01 angstrom with corresponding cavity temperatures of 6.3, 5.7 and 0.1 ^{0}C (above ambient temperature). We will now describe the stability of such an equilibria triplet:

#4672 - $15.00 US Received 17 August 2004; revised 16 September 2004; accepted 17 September 2004

1) Stable warm-equilibrium: In the first equilibrium (Fig. 1(b)) the cavity Lorentzian is on the right side of the pump line. This is a self-stable equilibrium since a small pump power decrease will reduce the cavity temperature and consequently the cavity wavelength will drift to the left; this will increase the absorbed power and hence will compensate for the pump reduction (an increase in pump power will cause a small compensation to the other direction).
2) Unstable warm- equilibrium: In the second equilibrium (Fig. 1(c)) the cavity Lorentzian is on the left side of the pump line. This equilibrium is unstable since a small reduction in the pump power will cause the cavity to cool down and the resonance wavelength to drift to the left. The subsequent reduced absorption will cause faster cooling and increased drift until the resonance reaches the trivial cold equilibrium solution described below.

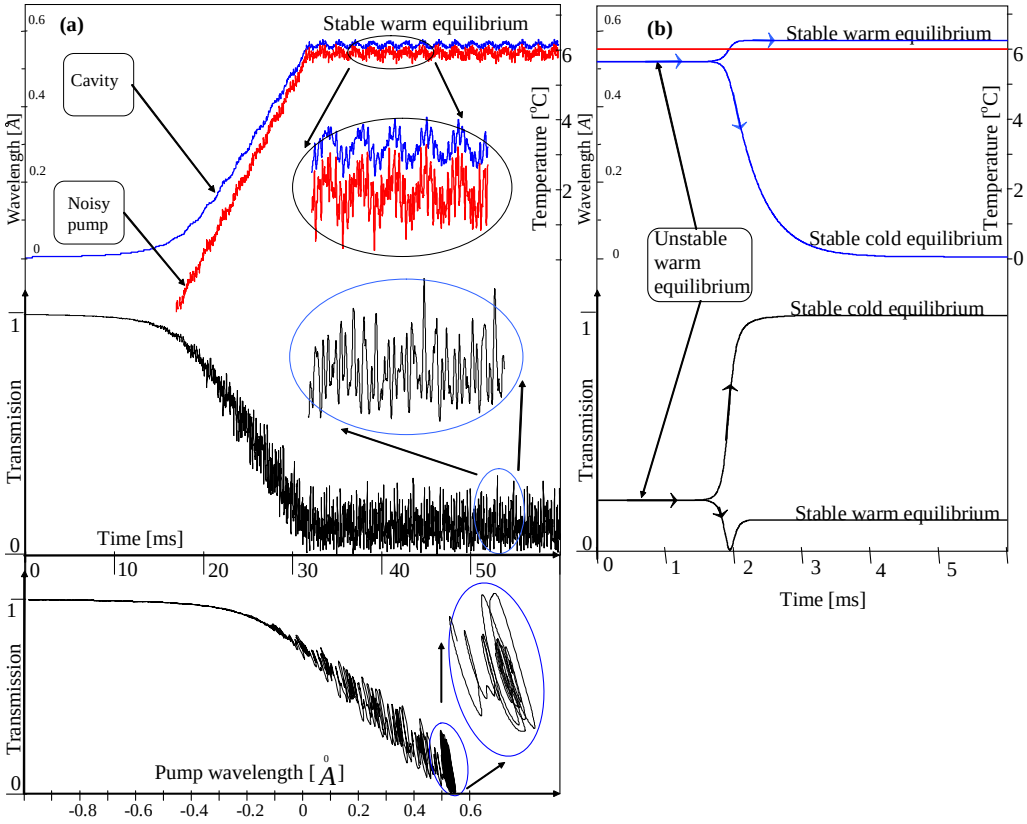

Fig. 4. Numerical calculation of dynamical noise response at equilibrium. (a) Warm stable-equilibrium: The stable warm equilibrium is reached by an upward wavelength scan, stopping at a pump wavelength of 0.56 angstrom above the cold resonance. In this equilibrium, the system overcomes Gaussian noise in the pump wavelength (with amplitude of one cavity width). The noise spectra is of random amplitude and spread Gaussianly in the Fourier space having FWHM of 100 KHz around the DC. (b) Unstable warm equilibrium: Starting in the unstable warm equilibrium (pump wavelength 0.56 angstrom and cavity thermal-drifted resonance 0.52 angstrom above the cold resonance), the smallest positive noise will take the system to the warm stable-equilibrium; while the smallest negative noise will take the system to the cold stable-equilibrium. Noise here is smaller than $1/10^{10}$ of the cavity FWHM. In this figure all parameters are as in Fig 1(b) (except for the pump wavelength), Figs. 2 and 3. All temperatures are relative to the ambient temperature and all wavelengths are relative to the cold cavity resonance.

3) Stable cold-equilibrium: In the third equilibrium (Fig. 3(d)) the cavity Lorentzian is far away from the pump line. Practically, no energy is absorbed by the cavity and hence this solution is not so interesting.

#4672 - $15.00 US Received 17 August 2004; revised 16 September 2004; accepted 17 September 2004

Practically speaking, reaching the warm stable-equilibrium is easiest by setting the pump to a wavelength smaller than the cold-cavity resonance and then starting to scan upward. Approaching from the other direction will pass through the unstable warm-equilibrium from which the system will almost immediately flip to one of the two stable-equilibria.

We will now demonstrate (first numerically and then experimentally) the system response to noise at different equilibria. When in stable equilibrium, the system will average out noise that is much faster than the thermal response time and will stay in quasi steady state when exposed to noise much slower than the thermal response time. both types of noise were included in our calculation.

In Fig 4(a) we show (numerically) that when a pump-cavity system is in a stable warm-equilibrium, it can overcome large fluctuations. We solve Eq. (4) for an up scan that takes the system reliably to the stable warm-equilibrium as noted above. The scan is stopped at a pump wavelength of 0.56 angstrom. It is apparent that large amplitude fluctuations are overcome and the system transmission remains low. On the other hand, the system cannot remain at the unstable equilibrium shown in Fig. 4(b) and noise that is 10 orders of magnitude smaller than in the former stable example (Fig. 4(a)) is enough to make the system flip to one of the two stable equilibria.

Cavity stability is demonstrated experimentally in Fig 5. Therein, we show an extremely slow up scan (Fig. 5 t<100s) that stops at a warm stable-equilibrium. In order to demonstrate experimentally that perturbations are compensated; we create a strong temporal perturbation in the pump power by knocking on the optical table (Fig. 5 inset); this leads to a change in the coupling efficiency. Despite the size and the relatively long duration of this perturbation, the system is stable again almost immediately after the perturbation stops

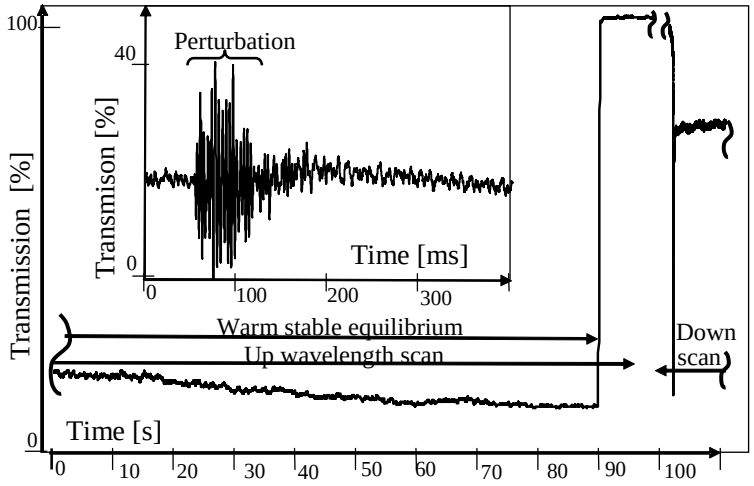

Fig. 5. The wavelength response for a slow scan (0.002 ${}^{0}A/s$) possesses a stable, warm equilibrium during the upward wavelength scan. A fast pass through resonance occurs during the downward wavelength scan (note that we zoom in here and show only a fraction of the wavelength scan). When in the warm stable equilibrium (in a region near 20 s in the scan), the system can recover from a perturbation as shown in the inset. We used a spherical cavity with a diameter of 0.26mm and $Q = 2\times10^{6}$.

On the other hand, as described theoretically above, when we down scan downward towards the resonance (Fig. 5, t>100s) then it is not possible to stay at the warm equilibrium**.** It is important to note here that while self stability can compensate for various types of noise, it can not compensate a continuous slow drift; as for example, a room temperature change of few degrees. Hence, it is useful to combine the thermal self stabilization with another control system [27] so that the control system will compensate for slow drifts and the thermal compensation will compensate the other noise.

#4672 - $15.00 US Received 17 August 2004; revised 16 September 2004; accepted 17 September 2004

4. Conclusions

Here we derived the equation for the dynamical thermal behavior of a microcavity and explain the microcavity line broadening and it's hysteretic wavelength response. As the thermal drift of the resonant (for a ~1 mW loaded microcavity) is typically more than 100 times the resonant width, thermal effects must be taken into account. Significantly, we showed theoretically and experimentally that a stable equilibrium exists in which perturbations are self compensated. This equilibrium is useful in both laboratory work and even potentially in commercial applications of these devices

Acknowledgments

We kindly thank Lee center for advance networking, and DARPA for their support. We thank Jacob Scheuer for the helpful discussion.

#4672 - $15.00 US Received 17 August 2004; revised 16 September 2004; accepted 17 September 2004